

## FREQUENCY-DEPENDENT SHORT-PERIOD EXPLOSION CODA AMPLITUDES IN NORTHERN EURASIA

Igor B. Morozov, Chaoying Zhang, and Elena A. Morozova

University of Saskatchewan

Sponsored by the National Nuclear Security Administration  
Office of Nonproliferation Research and Development  
Office of Defense Nuclear Nonproliferation

Contract No. DE-FC52-05NA26609

### **ABSTRACT**

Travel-time and magnitude-yield calibration of Northern Eurasia, which is largely aseismic, can be improved by using the large chemical and peaceful nuclear explosion (PNE) seismic data sets acquired by the Soviet deep seismic sounding (DSS) program. Eleven major data sets of this program have recently been digitized and have become available to nuclear test monitoring research. Although the PNEs have been already used in several monitoring studies, the chemical-explosions data sets are still incompletely explored. In the present study, we use inversion and numerical modeling to analyze the coda amplitude parameters and  $P$ -wave travel times from numerous DSS explosions, which could lead to a detailed empirical mapping of seismic properties within northern Eurasia.

For proper mapping of coda parameters, it is important to select a parameterization that reflects the fundamental physics and is stable in respect to unconstrained factors. We investigated two types of such parameterizations, namely the frequency-dependent coda attenuation  $Q_{\text{coda}}(f)$  and frequency-independent attenuation with geometric spreading ( $\gamma Q_{\text{coda}}$ ). By utilizing a newly developed, parallelized version of the one-dimensional (1-D) *reflectivity* program, we were able to model within the 0.2 to 10 Hz frequency band and to 800 sec times, which nearly covers the complete DSS time-frequency range. Several complexly layered velocity models related to the study area were tested.

The numerical modeling showed that for a fixed intrinsic  $S$ -wave  $Q$  of the crust, the resulting  $Q_{\text{coda}}(f)$  exhibited a strong positive frequency dependence. This spurious frequency dependence is due to a disregard of ray bending and other geometrical propagation effects and not related to model rheology. Notably, similar strong  $Q_{\text{coda}}(f) \propto f^{0.8-1.0}$  dependencies were observed in many PNE coda records and also in other areas. By contrast, coda amplitude inversion using the geometric-spreading model results in a stable spreading parameter,  $\gamma \approx -0.008$  and a frequency-independent  $Q_{\text{coda}}$  varying from  $\sim 2Q$  for  $Q = 300$  to  $\sim 1.2Q$  when  $Q = 1000$ . The variations in  $Q_{\text{coda}}(Q)$  as well as the fact that  $Q_{\text{coda}} > Q$  are consistent with a part of seismic coda energy propagating through the mantle. Tests for variations of the crustal velocity structure suggest that the  $Q_{\text{coda}}(Q)$  dependence is relatively stable, and therefore it can be used to invert for the intrinsic/scattering attenuation of the crust from coda measurements.

We have assembled a database of coda records from selected PNEs and chemical explosions and performed their inversion and preliminary interpretation based on the ( $\gamma Q_{\text{coda}}$ ) model. As in the modeling, parameter  $\gamma$  is relatively stable, whereas  $Q_{\text{coda}}$  shows variations that can be associated with tectonic structures. Crustal  $Q$  parameters are further mapped from the inverted modeled  $Q_{\text{coda}}(Q)$  dependence.

In order to further expand the DSS database, we have obtained earthquake recordings from several DSS PNE profiles. In the ongoing work, we are utilizing these data for coda magnitude analysis and derivation of empirical magnitude (apparent coda source spectra) relationships. Additionally, we present an update of our first-arrival travel-time calibration model for Northern Eurasia using the PNE as well as selected chemical-explosion records. These efforts should ultimately lead to a unified three-dimensional/two-dimensional (3-D/2-D) calibration model of Northern Eurasia, including travel times, stable coda magnitudes, and magnitude-yield relations. This model will bridge the gap between Europe, central Asia, the European Arctic, and eastern Siberia and provide additional calibration information for further studies in these areas.

Report Documentation Page				Form Approved OMB No. 0704-0188	
Public reporting burden for the collection of information is estimated to average 1 hour per response, including the time for reviewing instructions, searching existing data sources, gathering and maintaining the data needed, and completing and reviewing the collection of information. Send comments regarding this burden estimate or any other aspect of this collection of information, including suggestions for reducing this burden, to Washington Headquarters Services, Directorate for Information Operations and Reports, 1215 Jefferson Davis Highway, Suite 1204, Arlington VA 22202-4302. Respondents should be aware that notwithstanding any other provision of law, no person shall be subject to a penalty for failing to comply with a collection of information if it does not display a currently valid OMB control number.					
1. REPORT DATE <b>SEP 2007</b>		2. REPORT TYPE		3. DATES COVERED <b>00-00-2007 to 00-00-2007</b>	
4. TITLE AND SUBTITLE <b>Frequency-Dependent Short-Period Explosion Coda Amplitudes in Northern Eurasia</b>				5a. CONTRACT NUMBER	
				5b. GRANT NUMBER	
				5c. PROGRAM ELEMENT NUMBER	
6. AUTHOR(S)				5d. PROJECT NUMBER	
				5e. TASK NUMBER	
				5f. WORK UNIT NUMBER	
7. PERFORMING ORGANIZATION NAME(S) AND ADDRESS(ES) <b>University of Saskatchewan, Saskatoon, Saskatchewan, Canada, CA, 92093</b>				8. PERFORMING ORGANIZATION REPORT NUMBER	
9. SPONSORING/MONITORING AGENCY NAME(S) AND ADDRESS(ES)				10. SPONSOR/MONITOR'S ACRONYM(S)	
				11. SPONSOR/MONITOR'S REPORT NUMBER(S)	
12. DISTRIBUTION/AVAILABILITY STATEMENT <b>Approved for public release; distribution unlimited</b>					
13. SUPPLEMENTARY NOTES <b>Proceedings of the 29th Monitoring Research Review: Ground-Based Nuclear Explosion Monitoring Technologies, 25-27 Sep 2007, Denver, CO sponsored by the National Nuclear Security Administration (NNSA) and the Air Force Research Laboratory (AFRL)</b>					
14. ABSTRACT <b>see report</b>					
15. SUBJECT TERMS					
16. SECURITY CLASSIFICATION OF:			17. LIMITATION OF ABSTRACT <b>Same as Report (SAR)</b>	18. NUMBER OF PAGES <b>12</b>	19a. NAME OF RESPONSIBLE PERSON
a. REPORT <b>unclassified</b>	b. ABSTRACT <b>unclassified</b>	c. THIS PAGE <b>unclassified</b>			

## OBJECTIVES

Many seismic monitoring studies are based on properties of the seismic coda from earthquakes and explosions and, in particular, on its amplitude decay and attenuation. Short-period coda amplitude decays lead to the most stable estimates of source magnitudes (Phillips, 2004), and measured coda attenuation ( $Q$ ) is often related to crustal properties that are difficult to measure otherwise (Aki and Chouet, 1975). High-frequency (>5 Hz) codas from PNEs in the east European platform also led several researchers (Ryberg et al., 1995; Enderle et al., 1997; Morozov et al., 1998a,b; Ryberg and Wenzel, 1999; Morozov, 2001) to propose sharply contrasting models of small-scale heterogeneity of the uppermost mantle.

Despite its broad use in seismological practice, the causes of variations of coda  $Q$  with frequency are still not well understood. In many studies, strong frequency dependencies of coda  $Q$ , as well as body- and surface-wave  $Q$ , were documented. This dependence is commonly presented in a power-law form:

$$Q(f) = Q_0 \left( \frac{f}{f_0} \right)^\eta, \quad (1)$$

where  $f_0$  is some reference frequency often taken to equal 1 Hz (Aki and Chouet, 1975). Both  $Q_0$  and exponent  $\eta$  are considered constant within the frequency band of interest. Note that  $Q$  typically increases with frequency ( $\eta > 0$ ), and large values of  $\eta \sim 0.5$ -1 are not uncommon in  $Lg$   $Q$  and  $Lg$  coda  $Q$  studies (e.g., Nuttli, 1973; Hasegawa, 1985; Der et al., 1986; Campillo, 1987, 1990; Benz et al., 1997; Frankel et al., 1990; Mitchell and Cong, 1998; Mitchell et al., 1997, 1998; McNamara et al., 1996; McNamara, 2000; and Erickson et al., 2004). Visco-elastic rheological models were proposed to explain observations of frequency-dependent  $Q$  in Earth materials (Liu et al., 1976). Correlation to tectonics in North America suggested that active tectonic regions are generally characterized by low  $Q_0$  and high  $\eta$ , while stable cratons are generally characterized by higher  $Q_0$  and lower  $\eta$  (Erickson et al., 2004). However, in our PNE studies in the Siberian Craton, extremely high values of  $\eta \approx 1$  were found in combination with very high  $Q_0$  (Morozov et al., 2006). For  $\eta \approx 1$ , the coda amplitude decay becomes in fact frequency-independent, and this suggests a hypothesis that high apparent  $\eta$  could in fact indicate low attenuation and significant geometric spreading. An argument in favor of such an interpretation will be given below.

In coda measurements, its  $Q(f)$  value is derived from the following model of time-frequency dependent coda amplitudes:

$$A(t, f) = A_0(f) \exp \left( - \frac{\pi f}{Q(f)} t \right), \quad (2)$$

where  $t$  is the time after the primary arrival and  $A_0(f)$  is the coda spectrum at  $t=0$ . Note that the key assumption of model (2) is that the geometrical spreading of coda waves ( $\propto t^\zeta$  in Aki and Chouet, 1975) is compensated by the scattering volume increasing as the time  $t$  increases. Similarly, note that in surface wave studies (e.g., Erickson et al., 2004), frequency-dependent  $Q$  can be measured only by time-domain techniques, which also rely on compensation of geometrical spreading (Nuttli, 1973).

In this report, we show that observations of frequency-dependent coda  $Q$  may be related not to crustal rheology but to the chosen parameterization Eq. (2). Compensation of geometrical spreading in Eq. (2) should be relatively complete for local earthquake codas involving straight scattered rays and uniform scattering volumes (Aki and Chouet, 1975). However, at crustal-scale and regional distances, scattering tends to concentrate near the surface, and scattered waves consist of complex assemblages of diving, refracted, reflected, guided, and surface modes. Based on various assumptions about these modes and stochastic properties of the crust, several coda models can be used (e.g., Aki and Chouet, 1975; Sato and Fehler, 1998). In practice, however, with virtually any coda model, additional *ad hoc* distance and spectral corrections are required (Mayeda and Walter, 1996; Phillips et al., 2004). Here, we introduce such a correction by noting that an uncompensated (most likely, undercompensated) geometrical spreading  $G(t)$  should remain in the coda. Because it is only practical to seek a two-parameter coda description [similar to  $(Q_0, \eta)$  in Eq. (1)], we abandon the frequency dependence of  $Q_{\text{coda}}$  in relation (2) and approximate the geometrical spreading as  $\exp(-\gamma t)$ , yielding:

$$A(t, f) = A_0(f) \exp \left[ - \left( \gamma + \frac{\pi f}{Q_{\text{coda}}} \right) t \right], \quad (3)$$

where the geometric spreading (relaxation) parameter  $\gamma$  is measured in units of  $1/\text{time}$ . A similar expression for frequency dependence of surface wave attenuation was given by Dainty (1981). Note that the extreme case of  $\eta = 1$  [ $Q_{\infty}f$  in Eq. (2)] simply corresponds to geometrical spreading with low attenuation ( $Q_{\text{coda}} = \infty$ ) in relation (3).

Our objective below is to show that the  $(Q_0, \eta)$  description of frequency-dependent coda attenuation (and maybe also in other types of bulk crustal  $Q$ ) can be effectively and usefully replaced with  $(\gamma, Q_{\text{coda}})$ . The principal advantages of such a replacement are three-fold: 1) formula (3) does not rely on assumptions about geometrical spreading but empirically parameterizes it instead; 2) geometrical spreading and  $Q$  are explicitly separated; and 3)  $Q_{\text{coda}}$  becomes frequency-independent, in agreement with simple Newtonian solid-state mechanics, at least within the presently available data resolution. The somewhat puzzling increase of  $Q$  with frequency suggesting depletion of scatterers at shorter scale lengths becomes explained by geometrical spreading due to diving (among other) scattered waves. In addition, as our analysis of PNE profiles shows (see example below and Part II of this paper), parameter  $\gamma$  appears to be relatively stable across large areas, whereas  $Q_{\text{coda}}$  shows strong variability between different tectonic structures.

Below, we analyze the  $(Q_0, \eta)$  and  $(\gamma, Q_{\text{coda}})$  parameterizations of coda attenuation using numerical examples. We generate four finite-difference models of PNE coda wavefields resulting from realistic crustal and upper-mantle velocity models and test them for variations of crustal velocities and  $Q$ . As expected, the  $(Q_0, \eta)$  parameterization leads to strong spurious  $Q_{\text{coda}}(f)$  dependencies. Inversion of this  $Q_{\text{coda}}(f)$  for the true crustal  $Q$  could represent a non-trivial task. By contrast, in the  $(\gamma, Q_{\text{coda}})$  model, the values of  $\gamma$  can be predicted from the crustal structure, and  $Q_{\text{coda}}$  can be uniquely related to  $Q$  of the crust. Repeated for several types of velocity structures and crustal velocities, this modeling allows us to construct “calibration” dependences  $Q(Q_{\text{coda}})$  from numerical models and use them to invert the observed coda data for crustal properties in future research. In addition, we derive an approximate mapping of  $(\gamma, Q_{\text{coda}})$  parameters into  $(Q_0, \eta)$  and discuss the potential causes of observing low or high values of  $\eta$ . It appears that rather than  $\eta$  or  $Q_0$ , as an attribute of the velocity structure,  $\gamma$  could be a better factor differentiating between stable (cold) and active (hot) tectonic zones.

Overall, it appears that parameterization  $(\gamma, Q_{\text{coda}})$  is not only safer theoretically, but also provides the basis for inverting coda amplitudes for bulk crustal  $S$ -wave attenuation and for tying them to the tectonics. Because of its explicit separation of geometrical and attenuation effects, the approach is also likely to help in building more robust and transportable coda magnitudes and  $Q$ -based seismic regionalization.

## RESEARCH ACCOMPLISHED

We examine the effective frequency dependence of coda attenuation by numerically modeling the teleseismic  $P$  wave coda resulting from scattering of seismic energy from near-surface crustal heterogeneities. The use of near-surface crustal scatterers simplifies our computations, and it is also justified by the increased heterogeneity of the shallow crust and supported by several array observations (e.g., Greenfield, 1971; Dainty, 1985 and 1990; Bannister et al., 1990; Gupta et al., 1991) and previous coda modeling (Dainty and Schultz, 1995). The choice of the  $P$ -wave coda is due to several reasons (Morozov and Smithson, 2000): 1)  $S$ - and  $L_g$  phases are less pronounced in the PNE records; 2) their codas lie on top of the  $P$ -wave coda, complicating the observation and requiring their decomposition; and 3) the  $L_g$  phase is significantly more difficult to model accurately. Similarly, the Rayleigh wave ( $R_g$ ) decays quickly in near-surface sediments, and it is not viewed as a significant factor in coda formation (Dainty, 1985).  $R_g$  is not seen beyond  $\sim 200$  km in PNE records and is also difficult to reproduce numerically; consequently it is not examined here. The use of  $P$ -wave coda of arrivals at  $\sim 2900$  km from the source provides a sufficient coda time window before the onset of the  $S$ -wave phase.

**Crustal and coda attenuation.** It is important to differentiate between two different  $Q$  values used in this study. The intrinsic or elastic crustal attenuation describes the loss of seismic energy in the crust to internal friction, such as damping by fluids in cracks and pores or friction along grain boundaries. It is denoted by a  $Q$  value, where

$$Q = \frac{2\pi E}{\Delta E}, \text{ with } E \text{ being the energy and } \Delta E \text{ - the energy dissipation during one wave cycle (Aki and Richards,}$$

2002). By contrast,  $Q_{\text{coda}}$  measures the coda amplitude decay rate, determined from the decay slope of amplitude  $A$  versus time  $t$  from a semi-log plot of the seismic trace envelope in Eq. (2). By taking the natural logarithm:

$\ln A = \ln A_0 - \frac{\pi f}{Q_{\text{coda}}} t$ , we obtain a straight line with slope  $s = \frac{-\pi f}{Q_{\text{coda}}}$  in the  $(\text{time}, \ln A)$  domain. Thus, the

frequency-dependent  $Q_{\text{coda}}(f)$  is defined as:  $Q_{\text{coda}} = \frac{-\pi f}{s}$ , where slope  $s$  is measured from the logarithm of the seismic trace envelope.

**Numerical Coda Model.** The scattering model represents crustal heterogeneities as scatterers distributed within Earth's crust. The resultant scattered coda intensity  $U$  recorded at a receiver at time  $t$  is an integral over volume  $V$  containing all scatterers (Figure 1):

$$U(\vec{r}, t) = \int dt_s \iint_S d^2 \vec{r}_s \Psi(\vec{r}_s) U_{\text{source}}(\vec{r}_s, t_s) G(\vec{r} - \vec{r}_s, t - t_s). \quad (4)$$

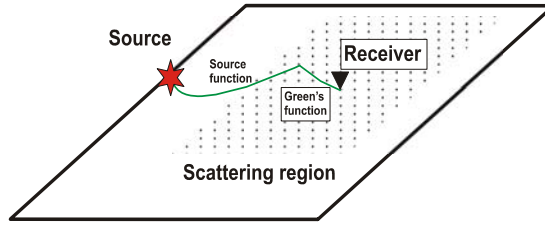


**Figure 1. Surface scattering model (Eq. 4). Seismic energy originates at the source, scatters from randomly and uniformly distributed surface points, and is detected at receiver. The source and Green's functions are simulated by 1-D reflectivity modeling.**

For a given coda time  $t$  and velocity of a particular scattered mode (e.g.,  $v = 2.9 - 3.5$  km/s for a scattered  $L_g$ ), contributions of scattered energy originate from an elliptical ring surrounding the receiver (Morozov and Smithson 2000). The scattering area within the ring increases with time due to its increasing radius and partly compensates the energy decay from the geometrical spreading. For example, for a plane of constant scattering potential and no intrinsic attenuation, coda energy would not decay, provided only surface-wave modes contribute to the scattered Green's function.

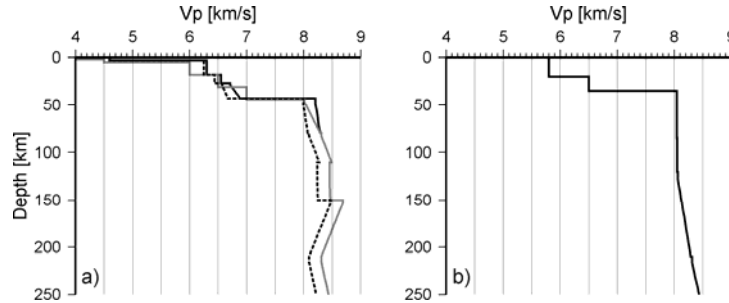


**Figure 2. Upper 250 km of 1-D  $V_p$  velocity models used in creation of synthetic seismograms. a) Models based on PNE Quartz results by Morozova et al. (1999): Quartz (solid black line), Warm Quartz (dotted black), and Complex Crust (gray); b) iasp91 model.**

Synthetic seismic sections created using the reflectivity method (Fuchs and Müller, 1971) were used as source and Green's functions in several 1-D crustal and upper mantle models (Figure 2). The original FORTRAN program by

K. J. Sandmeier was modified to handle larger computations, parallelized, and incorporated into our data processing system (SIA; Chubak and Morozov, 2006) allowing seamless filtering, inverting, saving, and plotting the results.

A detailed description of this tool can be obtained from the SIA web service:  
<http://seisweb.usask.ca/SIA/ps.php?doc=reflect>.

Computations were performed on a 66-processor 1.6-GHz Opteron cluster and produced 800-second, 3-component synthetic records sampled at 20-ms intervals and output at 10-km intervals from near-0 to 3500 km from the source. Modeling frequency band was 0.2–20 Hz using a “delta-function” source function suitable for spectral measurements. A sufficiently dense phase velocity spectrum was selected to avoid frequency aliasing during numerical mode summations. As with any implementations of the propagator matrix method (Aki and Richards, 2002), all *P*/*SV* mode conversions and multiples were accounted for in the modeling.

We used four different velocity models to compute the synthetics (Figure 2), including the global iasp91 model (Kennett and Engdahl, 1991), consisting of a simple three-layer crust and a mantle without strong gradients and low-velocity zones. However, the iasp91 model is too slow for platform areas of northern Eurasia, and the remaining three models were based on the detailed models derived from the NE profile Quartz and considered the best match for the study area (Mechie et al., 1993; Morozova et al., 1999). The “Quartz” model contains a 3-gradient layer crust overlain by a 3-km-thick sediment layer and complex mantle with low velocity zones at 110- and 210-km depths (Figure 2). Another “Complex Crust” model has a high-contrast, 5-layer crust with a somewhat exaggerated attenuative layer ( $Q_s = 10$ ) on its top and the Quartz mantle (Figure 2b). Model “Warm Quartz” (Figure 2a) was an attempt to simulate a high-heat flow regime in the Quartz model by applying a temperature-related negative velocity gradient within the crust (Christensen and Mooney, 1995). Note that all three Quartz-based models show more complex waveforms (including crustal  $L_g$  phases in addition to the *P* and *S* phases) compared with the iasp91 (Figure 2). In order to collect data on the sensitivity of the results to crustal velocities alone, we also repeated the Quartz simulations after applying  $\pm 5\%$  perturbations of crustal velocities.

Multiple simulations were performed for each model, with *P*- and *S*-wave quality factors for layers in the crustal part of the model set equal— $Q_p = 2Q$  and  $Q_s = Q$ , respectively, with values of  $Q$  ranging from 100 to 1000 to encompass the expected Earth’s whole-crust  $Q_s$  values. This range of  $Q_s$  corresponds to  $L_g$   $Q$  values of  $\sim 300$ –1000 measured from 19 Russian PNEs by Li et al. (submitted to the Bulletin of the Seismological Society of America [BSSA]) and extended to low- $Q$  values to investigate crustal effects. Mantle attenuation in each velocity model was fixed using the mantle  $Q_p$  values derived from *P*-wave Quartz PNE data (Morozov et al., 1998b). The teleseismic *P* coda was measured at 2900-km offsets to allow a significant time interval in which to perform the measurement before the onset of the  $P_g$  and *S* waves. Numerical evaluation of integral (4) was performed by using Monte-Carlo sampling in order to avoid spurious coherency that could be caused by spatial aliasing when using a regular integration grid. As above, the synthetic coda generation was implemented in an SIA tool sharing much of its libraries with other codes (<http://seisweb.usask.ca/SIA/ps.php?doc=syncoda>).

Using the resulting coda records, log-amplitude slope measurements were performed on coda envelopes in the manner of Morozov and Smithson (2000) (Figure 3). Both  $L_2$ - (root mean square [RMS]) and  $L_1$ -norm fitting (e.g., Aster et al., 2002) were tried, with uncertainties measured using 50% jack-knife resampling. Owing to large sampling volumes and stable coda envelopes, both the differences between the  $L_2$  and  $L_1$  norms and the corresponding slope uncertainties were negligible for the subsequent analysis.

**Modeling Results.** We performed measurements of the teleseismic *P*-wave codas for each of the four velocity models. Coda traces were band-pass filtered to center frequencies of 0.4, 0.79, 1.58, 3.16, 4.48, 6.32, 8.94, 12.6, and 17.8 Hz to examine the log-amplitude slopes as functions of frequency. Figure 4 shows the results for models Quartz and Complex Crust with  $Q_s = Q = 500$ .

In Figure 4, coda slope values show clear linear dependencies to about 7 to 10 Hz, after which the fidelity of modeling appears to drop, and the slopes flatten out (attenuation is replaced by frequency-independent

numerical noise of unclear nature). By fitting straight lines to the points within the 0 to 7 Hz range, we find that the intercepts at  $f = 0$  Hz are non-zero,  $\gamma \approx 0.8 \cdot 10^{-2}$ , and  $\gamma \approx 1.6 \cdot 10^{-2}$  for the two models and measure  $Q_{\text{coda}}$  from their slopes (see Eq. 3) as  $Q_{\text{coda}} \approx 800$  and 600, respectively. Note that  $\gamma$  is clearly positive in all cases considered here, indicating that the geometrical spreading is only partly compensated by surface scattering. Also note the flattening of  $\text{slope}(f)$  dependencies at higher frequencies due to the reduction in the signal/noise ratio and outliers at lower frequencies, most likely associated with tuning effects within the crustal layers (Figure 4).

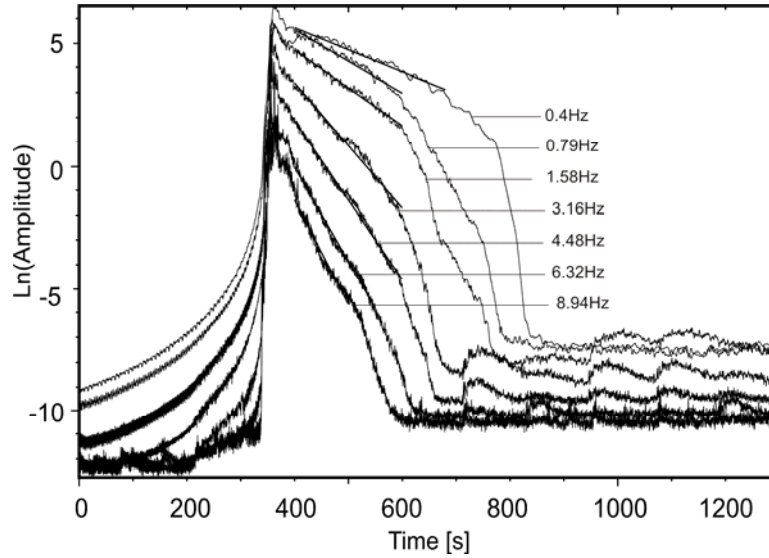


**Figure 3.** Log-amplitude synthetic coda for Quartz model at selected frequencies (labeled). Straight lines indicate the measured amplitude fits. Note the progressive change in coda shapes with increasing frequencies.

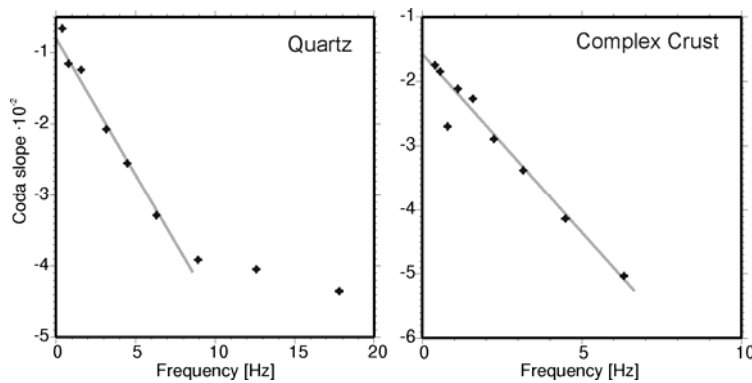


**Figure 4.** Measured log-amplitude coda slopes from models Quartz and Complex Crust with crustal  $Q_s = 500$ . Note the linearly decreasing (steepening) coda slopes with frequencies increasing to ~7-10 Hz. Solid gray lines indicate linear regressions using formula (3):  $\gamma = 0.8 \cdot 10^{-2}$  and  $Q_{\text{coda}} = 800$  for Quartz, and  $\gamma = 1.6 \cdot 10^{-2}$  and  $Q_{\text{coda}} = 600$  for Complex Crust models.

Alternatively, when converted to  $Q_{\text{coda}}$  by using Eq. (2), the values of slope result in frequency-dependent  $Q_{\text{coda}}(f)$  (Figure 5), which one could also fit using a dependence of type (1) with  $Q_0 \approx 250$  at 1 Hz and  $\eta \approx 0.5$  [see the discussion of conversion to  $(\eta, Q_0)$  below]. Although this interpretation could be acceptable within the synthetic or real data uncertainties, our model contains no mechanisms to support an *in situ* frequency-dependent attenuation. Therefore the observed  $Q_{\text{coda}}(f)$  (Figure 5) should be viewed as an “apparent” quantity or as an observational artifact.

By selecting linear  $\ln(A(t))$  dependencies (3) for each frequency, we found that the values of  $\gamma$  stayed approximately constant in all cases (values shown in labels in Figure 6). These observations were expected (see *Discussion*), as  $\gamma$  should principally depend on the crustal structure. By using these constant  $\gamma$ 's and for any frequency (Figure 6), the observed coda slopes can be transformed into the following ratios:

$$\alpha(Q) = \frac{Q_{\text{coda}}}{Q} = \frac{\pi f}{-Q \left( \frac{d \ln A(t, f)}{dt} + \gamma \right)} \quad (5)$$

Note that the resulting  $Q_{\text{coda}}/Q$  ratio is nearly frequency-independent, greater than 1, and approaches 1 for high  $Q$ . Because of these properties,  $\alpha(Q)$  can be tabulated and approximated from numerical modeling (lines in Figure 6) and utilized as a “calibration curve” for inverting the  $Q_{\text{coda}}$  observations for crustal  $Q$ . Interestingly, functions are very close (within  $\sim 0.2$  difference) for all three Quartz-based models, despite the strong difference in  $\gamma$  for the Complex Crust model (Figure 6). However, the  $\alpha(Q)$  for iasp91 model is strongly different from those for Quartz in its shape, values, and stability in respect to frequency variations (Figure 6).

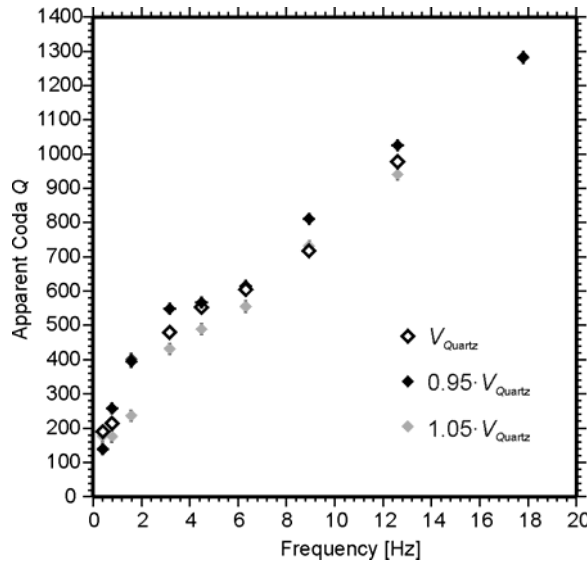


**Figure 5.** Measured log-amplitude coda slopes transformed to apparent coda  $Q_{\text{coda}}(f)$  according to relation (2). Note the strong frequency dependence ( $\eta \approx 0.5$ ) of  $Q_{\text{coda}}(f)$  despite the constant- $Q$  modeled crustal rheology.

Finally, both  $\gamma$  and the functional form of  $\alpha(Q)$  should depend on the velocity and density structures of the models. We tested this dependence by using four different types of models (Figure 2) and also by adding velocity perturbations to Quartz model. The results suggest that  $\gamma$  and  $\alpha(Q)$  indeed correlate with the structural model styles and crustal velocities, as will be further elaborated on in *Discussion*.

**Mapping the ( $\gamma, Q_{\text{coda}}$ ) parameterization to ( $Q_0, \eta$ ).** In most practical cases, the time-frequency amplitude decays  $A(f, t)$  can be satisfactorily matched in either ( $\gamma, Q_{\text{coda}}$ ) or ( $Q_0, \eta$ ) forms, and approximate mapping between them can be developed. Consider an attenuation process (e.g., coda) governed by Eq. (3) but parameterized by Eqs. (2) and (1). Therefore, for the time-dependent part of  $\ln A(f, t)$ , we have

$$\gamma + \frac{\pi f}{Q_{\text{coda}}} \approx \frac{\pi f}{Q_0 \left( \frac{f}{f_0} \right)^\eta} = q f^{1-\eta}, \quad (6)$$

where  $q$  is a constant. For a specific range of frequencies and coda times, transformation ( $\gamma, Q_{\text{coda}}$ )  $\rightarrow$  ( $Q_0, \eta$ ) can be found numerically by least-squares fitting the logarithm of Eq. (6):

$$\ln q + (1-\eta) \ln f \approx \ln \left( \gamma + \frac{\pi f}{Q_{\text{coda}}} \right), \quad (7)$$

and solving it for  $\ln q$  and  $(1-\eta)$ . The resulting ( $Q_0, \eta$ ) parameters for our numerical experiments are shown in Figure 7. Note that  $\eta$  is principally controlled by the  $\gamma Q_{\text{coda}}$  product, with  $Q_0 = Q_{\text{coda}}$  when  $\gamma = 0$  and decreasing with increasing  $\gamma$  (Figure 7). Thus, high  $\eta \approx 1$  should be expected in areas of low attenuation, with high geometric spreading, or when measurements are carried out at lower frequencies. Therefore, stable platforms (such as the Siberian Craton in eastern Russia) could exhibit high apparent frequency dependence of  $Q_{\text{coda}}$  simply on account of their high  $Q$ . More detail on this can be found in Morozov et al. (submitted to BSSA).

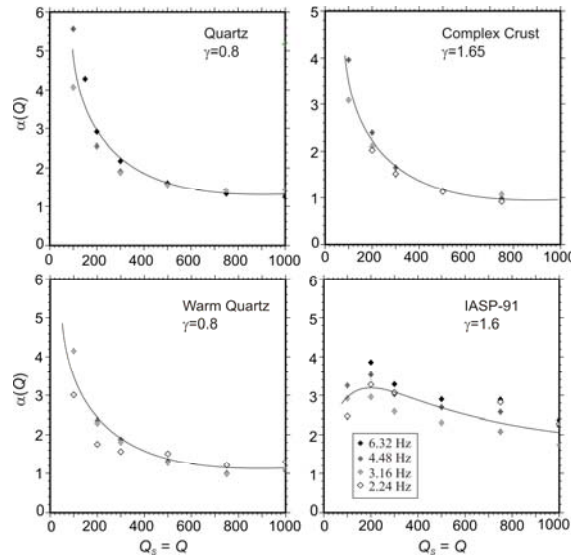


**Figure 6.**  $\alpha(Q_s)$  from Eq. (5) for the four models of this study and different frequencies (labeled symbols), obtained directly from coda slopes by using  $\gamma$  values in Eq. (3) shown in the labels. The lines represent the suggested empirical  $\alpha(Q_s)$  dependences for each velocity structure, picked by hand.

**PNE data example.** The use of  $(\gamma, Q_{\text{coda}})$  description allows us to resolve the following, recent, and hitherto puzzling observation from the PNE profiles. Within the east European platform, measurements from Quartz profile resulted in  $Q_{\text{coda}}(\sim 2 \text{ Hz}) = 380$  and  $Q_{\text{coda}}(\sim 5 \text{ Hz}) \approx 430$ , which was interpreted in the power-law form (1) as  $Q_{\text{coda}}(f) \approx 270 \cdot f^{0.3}$  (Morozov and Smithson, 2000). However, within the Siberian Craton (PNE Kimberlite-3), practically frequency-independent coda amplitude decays were observed, corresponding to  $Q_{\text{coda}}(f) \approx 1050 \cdot f^{1.0}$  (Morozov et al., 2006). Although the attenuation was expected to be low within the Siberian Craton, its strong frequency dependence is vastly different from the east European platform and is surprisingly high even for tectonically active areas (Erickson et al., 2004).

The explanation of the above in the  $(\gamma, Q_{\text{coda}})$  form is quite simple. From the Quartz-4 data, the logarithms of coda amplitudes can be interpreted by using  $\gamma \approx 0.75 \cdot 10^{-2} \text{ s}^{-1}$  and frequency-independent  $Q_{\text{coda}} \approx 850$ , with an estimated range of uncertainty of 780 to 960 (Figure 8). From Kimberlite-3 records,  $\gamma$  turns out to be nearly the same, and  $Q_{\text{coda}} \approx 2500 \pm 300$  (Figure 8). Thus, the Siberian Craton should occupy a region in the upper parts of the diagrams in Figure 7, where  $\eta \approx 1$ . Note that both values of  $\gamma$  also agree remarkably well with the numerical simulations based on Quartz velocity model data above (Figure 4). The values of  $Q$  within the Siberian Craton are very high, in agreement with observations of short-period  $P_g$  waves propagating to over 1600 km from the PNEs (Morozov et al., 2006). These are likely the longest-propagating short-period  $P_g$  observed anywhere on Earth.

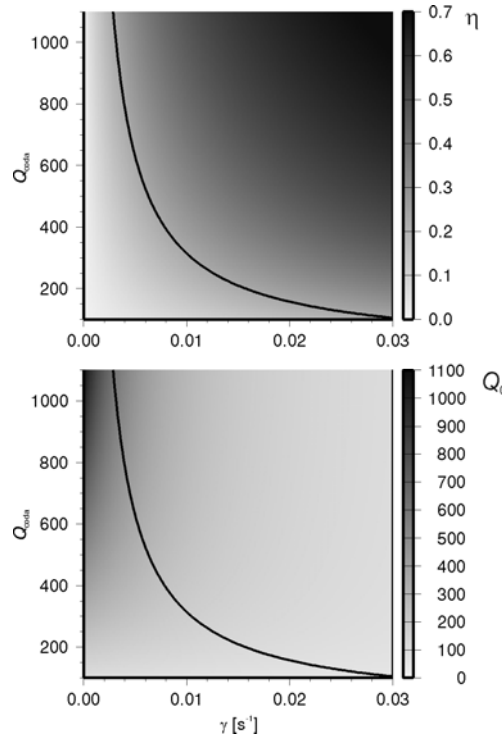


**Figure 7. Mapping of  $(\gamma, Q_{\text{coda}})$  to  $(Q_0, \eta)$  approximated for frequencies of 1 to 10 Hz. The hyperbolas drawn in both plots correspond to  $Q_{\text{coda}}\gamma = \pi 1 \text{ Hz}$ . Note that  $\eta$  increases with increasing  $Q_{\text{coda}}\gamma$ .**

## CONCLUSIONS AND RECOMMENDATIONS

Frequency-dependent attenuation often observed in regional coda measurements can be interpreted in two ways: by frequency-dependent coda  $Q_{\text{coda}}(f)$  or by means of effective, uncompensated geometrical

spreading ( $\gamma$ ) and frequency-independent coda attenuation ( $Q_{\text{coda}}$ ). The second of these alternatives offers a number of practical advantages: 1) it is better justified theoretically and does not require unusual crustal rheologies or inverted scaling properties; 2) its parameters can be quantitatively related to the *in situ* velocity/density ( $\gamma$ ) and attenuation ( $Q_{\text{coda}}$ ) crustal structures; 3) the resulting  $Q_{\text{coda}}$  appears to correspond to crustal  $Q_S$  and can be directly correlated to the observed  $Lg$   $Q$ ; 4) the frequency-independent parameters allow easier comparisons between different areas and studies; and 5) as stable characteristics, these parameters are likely to improve coda magnitude analysis and coda  $Q$  regionalization.

Frequency-dependent inelasticity due to spectral variations of scatterer density is certainly possible and likely to be present in Earth's crust. However, the objective of this paper was to show that it may not be as pervasive as suggested by many frequency-dependent  $Q$  observations. Within the available data quality, observations of apparent  $Q(f)$  at short periods could often be successfully explained by combinations of geometrical spreading (or turbidity in elastic scattering—Dainty, 1981) and frequency-independent attenuation. Separation of these physical parameters of the crust provides several insights for interpretation and allows linking the seismic velocity, structure, coda, and  $Lg$   $Q$  results. This conclusion is almost certainly the case with PNE data, and it may also apply to a variety of other seismic datasets (e.g., surface waves).

Numerical modeling of PNE coda wavefields argues strongly in favor of the new ( $\gamma$ ,  $Q_{\text{coda}}$ ) interpretation and illustrates the mechanisms leading to such an apparent  $Q(f)$ . The inverted  $Q_{\text{coda}}$  values can be systematically mapped into the true  $S$ -wave attenuation factors within the crust. By contrast, when interpreted using the traditional approach, the synthetic coda shows strong spurious frequency-dependent  $Q_{\text{coda}}$ .

PNEs in Russia in two different areas were found to have similar  $\gamma$  values, although strongly different  $Q_{\text{coda}}$ . We also suggest that parameter  $\gamma$  could provide a better, stable, and transportable discriminant for differentiating between tectonic types of the crust. From a limited preliminary example, this discriminant may relate to the presence of localized attenuative or scattering structures within the crust and be applicable to both North America and Northern Eurasia.

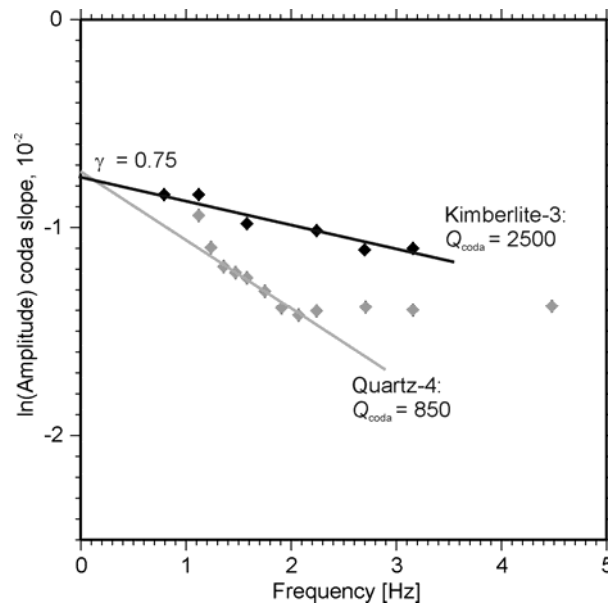


**Figure 8. Log-amplitude coda slopes in real data from PNEs Quartz-4 (recorded within the east European platform, at ~2600-km source-receiver offset; same data as in Morozov et al.,**

**2002) and Kimberlite-3 (recording within the Siberian Craton at ~1100-km offsets). Note the different  $Q_{\text{coda}}$  values (lines and labels), whereas the  $\gamma$  values are similar and close to those modelled. Also note that because of lower-magnitude source and longer recording distance, the usable frequency band is narrower for Quartz PNE records.**

## REFERENCES

- Aki, K. and B. Chouet (1975). Origin of coda waves: source, attenuation, and scattering effects, *J. Geophys. Res.* 80: 3,322–3,342.
- Aki, K., and Richards, P. G. (2002). *Quantitative Seismology*, Second Edition, University Science Books, Sausalito, CA.
- Aster, R., B. Borchers, and C. Thurber (2002). *Parameter Estimation and Inverse Problems*, preliminary edition.
- Bannister, S. G., E. S. Husebye, and B. O. Ruud (1990). Teleseismic P coda analyzed by three-component and array techniques: deterministic location of topographic P-to-Rg scattering near the NORESS array, *BSSA*, 80: 1969–1986.
- Benz, H., A. Frankel, and D. Boore (1997). Regional Lg attenuation in the continental United States, *Bull. Seism. Soc. Am.* 87: 600–619.
- Campillo, M. (1987). Lg wave propagation in a laterally varying crust and the distribution of the apparent quality factor in central France, *J. Geophys. Res.*, 92: 12604–12614.
- Campillo, M. (1990). Propagation and attenuation characteristics of the crustal phase Lg, *Pure Appl. Geoph.*, 132: 1–17.
- Christensen, N. I., and W. D. Mooney (1995). Seismic velocity structure and composition of the continental crust: A global view, *J. Geophys. Res.* 100: B7, 9761–9788.
- Chubak, G., and I. B. Morozov (2006). Integrated software framework for processing of geophysical data, *Computers & Geosciences* 32: 767–775.
- Dainty, A. M. (1981). A scattering model to explain seismic Q observations in the lithosphere between 1 and 30 Hz, *Geophys. Res. Lett.* 8: 1126–1128.
- Dainty, A. M. (1985). Air Force Geophysical Laboratory Report, AFGL-TF-86-0218.
- Dainty, A. M. (1990). Studies of coda using array and three-component processing, *PAGEOPH*, 132: 221–244.
- Dainty, A. M. and C. A. Schultz (1995). Crustal reflections and the nature of regional P coda, *Bull. Seismol. Soc. Am.*, 85: 851–858.
- Der, Z. A., A. C. Lees, and V. F. Cormier (1986). Frequency dependence of Q in the mantle underlying the shield region of Eurasia, Part III: The Q-model, *Geophys. J. R. Astr. Soc.* 87: 1103–1112.
- Enderle, U., M. Titgemeyer, M. Itzin, C. Prodehl, and K. Fuchs (1997). Scales of structure in the lithosphere - Images of processes, *Tectonophysics*, 275: 165–198.
- Erickson, D., D. E. McNamara, and H. Benz (2005). Frequency-dependent Lg Q within the continental United States, *Bull. Seism. Soc. Am.* 94: 1630–1643.
- Frankel, A., A. McGarr, J. Bicknell, J. Mori, L. Seeber, and E. Cranswick (1990). Attenuation of high-frequency shear waves in the crust: measurements from New York state, South Africa, and southern California, *J. Geophys. Res.* 95: 17441–17457.
- Fuchs, K., and G. Müller (1971). Computation of synthetic seismograms with the reflectivity method and comparison with observations, *J. R. Astronom. Soc.* 23: 417–433.
- Greenfield, R. J. (1971). Short-period P-wave generation by Rayleigh-wave scattering at Novaya Zemlya, *JGR* 76: 7988–8002.
- Gupta, I.N., T. W. McElfresh, and R. A. Wagner (1991). Near-source scattering of Rayleigh to P in teleseismic arrivals from Pahute Mesa (NTS shots, in: Taylor, S. R., H. J. Patton, and P. G. Richards (Eds.), *Explosion Source Phenomenology*, *AGU Geophys. Monograph* 65: 151–160.
- Hasegawa, H. S. (1985). Attenuation of Lg waves in the Canadian Shield, *Bull. Seism. Soc. Am.* 75: 1569–1582.

- Kennett, B. L. N. and R. Engdahl (1991). Traveltimes for global earthquake location and phase identification, *Geophys. J. Int.* 105: 429–465.
- Li, H., I. B. Morozov, and S. B. Smithson (submitted to *Bull. Seism. Soc. Am.*) Mapping Lg Q at 1-3 Hz in Northern Eurasia using nuclear-explosion profiles.
- Liu, H. P., Anderson, D. L., Kanamori, H. (1976). Velocity dispersion due to anelasticity: implications for seismology and mantle composition, *Geophysical Journal of the Royal Astronomical Society* 47: 41–58.
- Mayeda, K., and W. R. Walter (1996). Moment, energy, stress drop, and source spectra of western United States earthquakes from regional coda envelopes, *J. Geophys. Res.* 101: 11195–11208.
- McNamara, D. E. (2000). Frequency-dependent Lg attenuation in south-central Alaska, *Geophys. Res. Lett.* 27: 3949–3952.
- McNamara, D. E., T. J. Owens, and W. R. Walter (1996). Propagation characteristics of Lg across the Tibetan Plateau, *Bull. Seism. Soc. Am.* 86: 457–469.
- Mechie, J., A. V. Egorkin, K. Fuchs, T. Ryberg, L. Solodilov, and F. Wenzel (1993). P-wave velocity structure beneath northern Eurasia from long-range recordings along the profile Quartz, *Phys. Earth Planet Inter.* 79: 269–286.
- Mitchell, B. J. and L. Cong (1998). Lg coda Q and its relation to the structure and evolution of continents: a global Perspective, *Pure Appl. Geophys.* 153: 655–663.
- Mitchell, B. J., Pan, Y., Xie, J., Cong, L. (1997). Lg coda Q variation across Eurasia and its relation to crustal evolution, *J. Geophys. Res.* 102: 22767–22779.
- Morozov, I. B. (2001). Comment on “High-frequency wave propagation in the uppermost mantle” by T. Ryberg and F. Wenzel, *J. Geophys. Res.* 106: 30,715–30,718.
- Morozov, I. B., and S. B. Smithson (2000). Coda of long-range arrivals from nuclear explosions, *Bull. Seism. Soc. Am.* 90: 929–939.
- Morozov, I. B., E. A. Morozova, and S. B. Smithson (1998a). On the nature of the teleseismic Pn phase observed in the recordings from the ultra-long profile “Quartz”, Russia, *Bull. Seism. Soc. Am.* 88: 62–73.
- Morozov, I. B., E. A. Morozova, S. B. Smithson, and L. N. Solodilov (1998b). 2-D image of seismic attenuation beneath the Deep Seismic Sounding profile “Quartz”, Russia, *Pure and Applied Geoph.* 153: 311–348.
- Morozov, I., Morozova, E., Zhang, C. Chubak, G., Phillips, W. S. and Lipovetsky, I. (2006). Magnitude-yield and travel-time calibration of northern Eurasia using deep seismic sounding datasets, in *Proceedings of the 28th Seismic Research Review: Ground-Based Nuclear Explosion Monitoring Technologies*, LA-UR-06-5471, Vol. 1, pp. 130–140.
- Morozov, I. B., C. Zhang, J. N. Duenow, E. A. Morozova, and S. B. Smithson (2007). Frequency dependence of regional coda Q: Part I. Numerical modelling and an example from Peaceful Nuclear Explosions,” submitted to BSSA.
- Morozova, E. A., I. B. Morozov, S. B. Smithson., and L. N. Solodilov (1999). Heterogeneity of the uppermost mantle beneath Russian Eurasia from the ultra-long range profile QUARTZ, *J. Geophys. Res.* 104: (B9), 20,329–20,348.
- Nuttli, O. W. (1973). Seismic wave attenuation and magnitude relations for eastern North America, *J. Geophys. Res.*, 78, 5212–5218.
- Phillips, W. S., H. J. Patton, S. R. Taylor, H. E. Hartse, and R. E. Randall (2004). Calibration for coda based magnitude and yield, in *Proceedings of the 26th Seismic Research Review: Ground-Based Nuclear Explosion Monitoring Technologies*, LA-UR-06-5471, Vol. 1, pp. 449–456.
- Ryberg, T., and F. Wenzel (1999). High-frequency wave propagation in the uppermost mantle, *J. Geophys. Res.*, 104, 10,655–10,666.
- Ryberg, T., K. Fuchs, A. V. Egorkin, and L. Solodilov (1995). Observations of high-frequency teleseismic Pn on the long-range Quartz profile across northern Eurasia, *J. Geophys. Res.* 100: 18151–18163.
- Sato, H., and M. Fehler (1998). *Seismic Wave Propagation and Scattering in the Heterogeneous Earth*, Springer-Verlag, New York.